A Statistical Framework for the Sensitivity Analysis of Radiative Transfer Models

Robin D. Morris, *Member, IEEE*, Athanasios Kottas, Matthew Taddy, Roberto Furfaro, and Barry D. Ganapol

Abstract—Process models are widely used tools, both for studying fundamental processes themselves and as elements of larger system studies. A radiative transfer model (RTM) simulates the interaction of light with a medium. We are interested in RTMs that model light reflected from a vegetated region. Such an RTM takes as input various biospheric and illumination parameters and computes the upwelling radiation at the top of the canopy. The question we address is as follows: Which of the inputs to the RTM has the greatest impact on the computed observation? We study the leaf canopy model (LCM) RTM, which was designed to study the feasibility of observing leaf chemistry remotely. Its inputs are leaf chemistry variables (chlorophyll, water, lignin, and cellulose) and canopy structural parameters (leaf area index, leaf angle distribution, soil reflectance, and sun angle). We present a statistical approach to the sensitivity analysis of RTMs to answer the question previously posed. The focus is on global sensitivity analysis, studying how the RTM output changes as the inputs vary continuously according to a probability distribution over the input space. The influence of each input variable is captured through the "main effects" and "sensitivity indices." Direct computation requires extensive computationally expensive runs of the RTM. We develop a Gaussian process approximation to the RTM output to enable efficient computation. We illustrate how the approach can effectively determine the inputs that are vital for accurate prediction. The methods are applied to the LCM with seven inputs and output obtained at eight wavelengths associated with Moderate-resolution Imaging Spectroradiometer bands that are sensitive to vegetation.

Index Terms—Gaussian process (GP), main effects, Moderate resolution Imaging Spectroradiometer (MODIS), radiative transfer model (RTM), sensitivity analysis, sensitivity index.

I. INTRODUCTION

THE ACCURATE estimation of the properties of the biosphere is critical for our understanding of the Earth's coupled system. The atmosphere, oceans, and land comprise

R. D. Morris is with the Universities Space Research Association-Research Institute for Advanced Computer Science, Mountain View, CA 94041 USA, and also with the Department of Applied Mathematics and Statistics, University of California, Santa Cruz, CA 95064 USA (e-mail: rdm@riacs.edu).

A. Kottas is with the Department of Applied Mathematics and Statistics, University of California, Santa Cruz, CA 95064 USA.

M. Taddy is with the Graduate School of Business, University of Chicago, Chicago, IL 60611 USA.

R. Furfaro is with the Department of Aerospace and Mechanical Engineering, University of Arizona, Tucson, AZ 85721 USA.

B. D. Ganapol is with the Department of Aerospace and Mechanical Engineering and the Department of Hydrology and Water Resources, University of Arizona, Tucson, AZ 85721 USA.

Color versions of one or more of the figures in this paper are available online at http://ieeexplore.ieee.org.

Digital Object Identifier 10.1109/TGRS.2008.2002026

a complex coupled dynamical system and the valid statistical prediction of the properties of this system, and its changes, require inputs that are both accurate and have their uncertainties accurately quantified.

The study of the biosphere is dependent on models—mathematical abstractions of the systems themselves, which are sufficiently simplified to allow for mathematical or computational analysis in reasonable amounts of time. The study of these models can give important information about the systems being modeled, but shortcomings in the models, where they differ from reality, must not be overlooked. Models will have limitations due to the modeling philosophy chosen—the set of simplifying assumptions used by the scientist. Indeed, modeling uncertainty comes from a combination of the ignorance of natural variability and the impossibility of precisely modeling the physical phenomena being studied.

The behavior of these models with respect to their inputs is the subject of this paper. Analyzing the uncertainty characteristics of a model is a crucial first step in the use of the model for prediction and inversion. It gives information about the influence of the inputs, both individually and in groups, on the model output and can give information as to the potential of successfully performing model inversion.

In many cases, the model inputs are not easily observable. Instead, the model outputs are measured, and the model inputs must be inferred. Global models require global observation as inputs, and the only effective method for making routine global measurements is via sensors mounted on orbiting satellites. Typically, however, satellite-mounted sensors do not measure directly the quantity of interest. Passive visible/near infrared sensors measure upwelling radiation, and it is from these measurements that the biospherical parameters of interest must be inferred.

This inference process is complex. It is the inversion of the process of sunlight passing through the atmosphere, being reflected off vegetation on the ground, and then passing again through the atmosphere before being detected by the satellite-mounted sensor. The dominant sources of uncertainty in this scenario are the uncertain process models that enter the estimation. The uncertainty due to the process models will almost certainly be much larger than the uncertainty due to noise in the sensor [1]. The Moderate resolution Imaging Spectroradiometer (MODIS) [2] has an SNR of between 74 and 910 in the near infrared bands [3] and is radiometrically very well calibrated in other bands [4], [5]. In the brief outline aforementioned, we have two models, one for the propagation of light through the atmosphere and the second for the reflection of light by the vegetation on the ground. It is the uncertainty

characteristics of the second of these process models that we will analyze in this paper.

Analyzing, quantifying, and reporting the uncertainty in remote sensed data products is of great importance. It is the only way in which the uncertainty of further analyses using these data products as inputs can be quantified. Analyzing the source of the data product uncertainties can identify where the models must be improved or where better input information must be obtained. Both of these aspects are known; the editorial for the Special Issue on Global Land Product Validation [6] wrote:

> users need access to quantitative information on product uncertainties

and that

> [m]aking quantified accuracy information available to the user can ultimately provide developers the necessary feedback for improving the products.

The work in this paper is intended to contribute to this larger goal. We provide tools to allow model builders to better analyze the characteristics of the models that will subsequently be used for inversion. Developments of the tools we provide here will also allow for the characterization of the uncertainties in the inverse process.

There has been significant work toward the goals outlined above, but there is still much to be done. For example, the current MODIS Leaf Area Index (LAI)/fraction of Photosynthetically Active Radiation algorithm has been improved continuously since the satellite's launch. The main improvements have been in the use of a better biome map (reducing the uncertainty in that input), improvements in atmospheric correction, and improved models of surface reflectance from different biomes [7].

These improvements have reduced the uncertainty in the resulting data product, but have not necessarily improved the quantification of the uncertainties and have not specifically addressed the statistical identification of the sources of the uncertainties. Here, we will address one aspect of this overall process. Models of surface reflectance are typically radiative transfer models (RTMs). We analyze in detail the effects of the inputs to an RTM in terms of the sensitivity of the RTM's output to each of the inputs. Specifically, we analyze the leaf canopy model (LCM) RTM [8], used as a surrogate for the RTM used as the basis for the MODIS production algorithm [9]. See Section II for a discussion of the LCM. In Section III, we use and develop methods from the statistical literature on sensitivity analysis [10] to compute the main effects, which graphically show the relative importance of each input on the RTM output, and the sensitivity indices, which give a measure of the expected amount by which the uncertainty in the output would be reduced if the true value of the input was known.

A 1999 paper, [11], discussed the state of sensitivity analysis in the remote sensing and geoscience domains. At that time, the analyses were typically very basic, looking only at one variable at a time, and based around a fixed operating point. A number of suggestions as to better methods were made, principally the Fourier Amplitude Sensitivity Test [10]. This suggestion does not seem to have been adopted—the number of papers that cite [11] is small, and the number that adopt the suggestions,

smaller still. For example, [12] uses ideas from the design of experiments, but does not compute sensitivity indices. While discussing sensitivity indices, the analysis in [13] is based on local sensitivity computations. In [14], sensitivity indices are computed, but the methods used required large numbers of model runs. In this paper, we give explicit, computationally efficient methods for computing the main effects and sensitivity indices, as part of a global sensitivity analysis.

Computing the main effects and sensitivity indices requires the evaluation of multidimensional integrals over the input space of the model. Evaluating RTMs can be computationally expensive, and therefore, standard numerical integration methods (e.g., multidimensional quadrature or Monte Carlo integration) would be computationally prohibitive in terms of the number of times the RTM would have to be run. Instead, we adopt the approach of approximating the RTM by a Gaussian process (GP) model [15]–[17], a technique known in the statistical literature as *emulation*. A GP provides a very flexible nonparametric function approximation that has found wide application as a replacement for neural networks [15]. Early work involving GP response-surface approximations for the analysis of computer experiments includes [18]–[20]. We refer to [21] for background and further references. The GP model approximation can be constructed using a comparatively small number of carefully chosen RTM evaluations. See Section IV. Using the GP approximation instead of the actual RTM will introduce uncertainty into the evaluation of the main effects and the sensitivity indices, but this can also be quantified [22]. See Section V. The GP emulator, being a fully specified statistical model, is amenable to further analysis in ways that a set of sample responses of an RTM, or even the implementation of the RTM as a piece of software, is not. It allows for calibration and validation of the model in a principled statistical manner and as the likelihood in a statistical treatment of the model inversion. See [23], [24], and Section VII. The GP emulator provides a unifying framework for this and other problems.

Finally, in Section VI, we present the main effects and sensitivity indices for the LCM RTM and show how they enable the identification of the relative importance of each input to the model output. This also gives information as to how well these inputs can be predicted from observations of the model output at different wavelengths.

II. COUPLED LEAF-CANOPY RTM

Over the past decade, in collaboration with the Ecosystem Science and Technology Branch at NASA Ames, the Vegetation Modeling Transport Group (University of Arizona) has developed a coupled Leaf-Canopy Model (LCM) in order to capture the essential biophysical processes associated with the interaction between light and vegetation [8]. LCM was developed to provide a tool to aid in remote sensing as applied to ecosystem dynamics in support of the TERRA platform, and it is specifically used to investigate the feasibility of observing chemistry remotely. The model combines two different RTMs, one at leaf level (LEAFMOD) and one at canopy level [CANopy Model (CANMOD)] to predict the radiative regime inside the vegetation canopy under consideration.

LEAFMOD [25] is the model that simulates the radiative regime inside the single leaf. From a morphological point of view, the leaf element is an extremely complex and rich object. Any model that attempts to describe each single interaction process for the light moving in such a medium will face this enormous complexity. The strength of the LEAFMOD algorithm is its simplicity through natural averaging. The model relies on the fact that, while light is moving in a complicated medium, natural averaging occurs in such way that the simpler assumption of isotropic scattering and uniform absorption seems to capture the transport effects. Moreover, the model has the ability to include chemistry as a key element dominating the absorption process. Different concentrations of chlorophyll, water, lignin, and cellulose can be specified to model the optical properties of the single leaf species. The model is calibrated over the LOPEX leaf species archive [26], where experimental leaf property data are stored. The calibration occurs in the sense that the optical properties required by the canopy model are retrieved through a procedure that uses the LOPEX archive as input data.

Although LEAFMOD has been specifically designed and implemented to be coupled with the canopy model (CANMOD, see the following), it can also be used as a stand-alone module to describe the radiative transfer of photons within leaf media as functions of their morphological structure and biochemical signature. In early deterministic models, two-stream models were used to determine the radiative transfer within leaf structures. The so-called Kubelka–Munk (KM) theories [27] treat the leaf as a plane parallel medium, tacitly assume the scattering to be nearly isotropic, and assume weak volume absorption within leaves. By modeling the transport of photons as a diffusion process, the computed radiance is subject to large errors in optically thin media and/or in highly absorbing regions [28]. To overcome some of the difficulties associated with KM theories, PROSPECT [29] was established. Within the PROSPECT framework, the leaf is assumed to be modeled as a sequence of transparent plates, each assumed to be rough Lambertian reflectors. Each plate defines the optical properties of the interior of the leaves. Scattering is described by a spectral index of refraction and a parameter describing the leaf mesophyll structure. The absorption coefficients for leaf water and pigments are generally fitted using experimental data, i.e., leaf reflectance and transmittance. By contrast, LEAFMOD relies on rigorous first principles, i.e., the balance of photons. LEAFMOD's advantage stems from the fact that the overall leaf biochemistry can be easily specified and the scattering coefficient calibrated via experimental data and direct model inversion [30].

The CANMOD algorithm [8], [31] takes the information coming from LEAFMOD regarding the single leaf characteristics (transmittance and reflectance) and, together with canopy structural parameters [LAI and leaf angle distribution (LAD)], soil reflectance, and sun angle inclination, computes, at any given wavelength, the radiative regime within and at the top of the canopy by solving a radiative transfer equation. The strengths of the model are simplicity and the ability to take into account leaf chemistry, which is important to properly describe the light absorption environment.
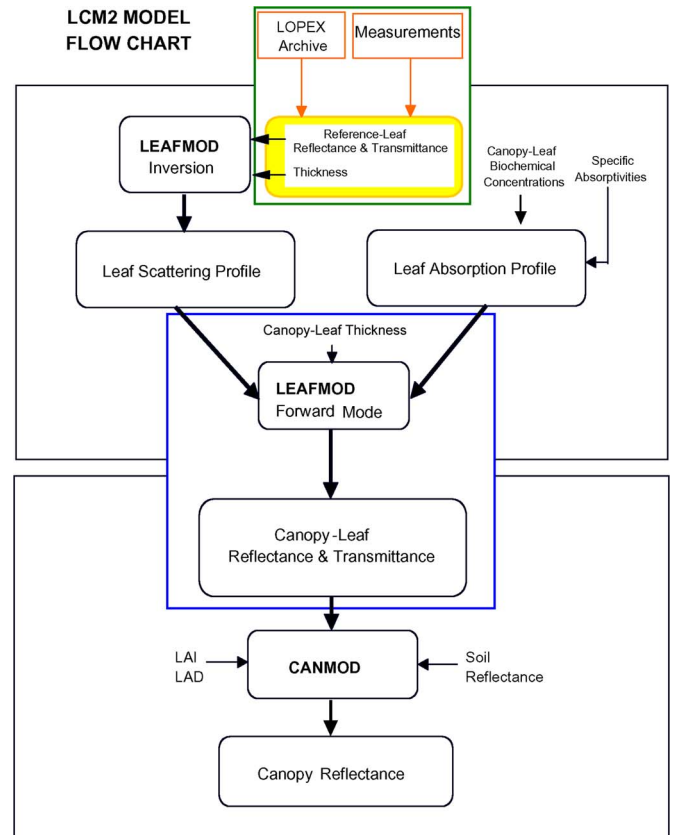
Fig. 1.　LCM flow chart.

Fig. 1 shows a flowchart that demonstrates the operation of the coupled algorithm. The algorithm can be explained as follows. The first module uses LEAFMOD in the forward and inverse modes to compute the leaf optical properties (i.e., leaf reflectance and transmittance). The second module uses the CANMOD forward mode to compute the spectral canopy hemispherical reflectance factor. The code requires the specification of the input parameters. In addition to the parameters listed in Table I, the model also takes as input wavelength (between 400 and 2100 nm), canopy architecture (LAD) and the sun angle. CANMOD is able to handle four discrete typologies of LAD, namely, planophile (leaves mainly horizontal), erectophile (leaves mainly vertical), plagiophile (leaves mainly at 45°), and extremophile (leaves mainly both horizontal and vertical). LAD is determined largely by knowledge of the biome. Its inference from observational data is difficult [32].

Note that the soil reflectance depends on the wavelength. Indeed, usually, the spectral soil reflectance is specified depending on the type of soil of interest. We assumed a typical visible/near infrared spectrum for a dry soil, and we considered a multiplicative brightness parameter varying between 0.3 and 1.3 (see Table I) to account for the possible variations of the background (soil) reflectance level [33]. This multiplicative parameter is assumed to be wavelength independent.

Once the leaf type is specified, the LOPEX database contains the measured leaf optical properties for the leaf of interest. Nevertheless, we can tune the canopy by considering leaves that are of the same type but with different biochemistry and thickness. This gives the code great flexibility in modeling the effect of

TABLE I
RANGES OF VALUES OF THE INPUTS TO THE LCM. LAI AND WATER
FRACTION ARE DIMENSIONLESS. THE SOIL PARAMETER IS
MULTIPLIED BY A STANDARD SOIL SPECTRUM. SEE TEXT

input	min	max
LAI	0	8
chlorophyll ($\mu g/cm^2$)	0	100
water fraction	0.1	0.8
protein (g/cm^2)	0.0001	0.001
lignin/cellulose (g/cm^2)	0.0001	0.006
thickness (cm)	0.001	0.01
soil	0.3	1.3

biochemistry on the overall canopy reflectance. The algorithm begins by analyzing the leaf under consideration. Assume, for example, that the canopy of interest is a maple canopy. The LOPEX database is accessed to retrieve the measured spectral reflectance and transmittance for a nominal maple leaf. Note that, as before, because the wavelength is set, reflectance and transmittance for the nominal leaf are selected for the specific wavelength of interest. The LEAFMOD inverse mode accepts the reflectance and transmittance and retrieves scattering and absorption coefficients. It is assumed that, to first order, the scattering depends on the anatomical structure of the leaf, whereas the absorption depends only on the biochemical components [25]. Thus, the scattering coefficient for maple leaves is assumed to be the same, and it is retained. A new maple leaf having the biochemical components and thickness specified by the inputs is constructed, retaining the same scattering coefficient and constructing the new absorption coefficient for the wavelength of interest. Both absorption and scattering coefficients are fed to the LEAFMOD forward mode to compute the reflectance and transmittance of the desired leaf, i.e., the leaf with thickness, water, chlorophyll, lignin, and protein specified by the inputs. Reflectance and transmittance are fed to the second module together with LAI, LAD, soil reflectance, and sun angle to compute the hemispherical reflectance.

III. SENSITIVITY ANALYSIS

Sensitivity analysis aims to determine how the variation in the output of a model can be apportioned among the inputs [21, Ch. 7]. That is, it attempts to determine how much of the variation seen in the output is due to variation in each of the inputs. The type of sensitivity analysis we are interested in here is *global* statistical sensitivity analysis, looking at how the output changes as all the inputs vary continuously, rather than the more common *local* derivative-based sensitivity analyses, which look at how the output changes as the inputs are each varied about a fixed point [34]. Clearly, this latter type of analysis will give limited information about how the output varies for substantial changes in the inputs.

How the inputs vary is determined by a probability distribution that defines the expected distributions of the inputs. Using v to denote the vector of model inputs, this distribution is $H(v)$. The actual form of this distribution is problem dependent and dependent on the amount of knowledge available about each input variable. It may be that, for some inputs, all that can be given is a physically plausible range (e.g., water fraction is limited to the range 0–1), whereas for others, a more precise

distribution may be known (e.g., the distribution of leaf thickness for a particular tree type may be known from field measurements). The distribution $H(v)$ also encodes correlations between variables that are known to vary together. The authors in [33] give truncated Gaussian distributions for the variables in Table I. In this paper, we use the simpler formulation of independent uniform distributions over the ranges given in Table I for each input variable.

A. Main Effects

Denote the response of the model to input v as $y = f(v)$. The function $f(v)$ can be decomposed as

$$y = f(v) = E(Y) + \sum_{i=1}^{d} z_i(v_i) + \sum_{i<j} z_{i,j}(v_i, v_j) + \cdots$$
$$+ z_{1,2,\ldots,d}(v_1, v_2, \ldots, v_d) \quad (1)$$

where $v = (v_1, \ldots, v_d)$ is d-dimensional (with $d = 7$ in our sensitivity analysis of the LCM). The first term is the expected value of $f(v)$, i.e.,

$$E(Y) = \int\limits_{v_j, j=1,\ldots,d} f(v) dH(v)$$

and the next d terms are the *main effects*, given by

$$z_i(v_i) = E(Y|v_i) - E(Y)$$
$$= \int\limits_{v_{-i}} f(v) d(v_{-i}|v_i) - E(Y) \quad (2)$$

where v_{-i} denotes all the elements of v except v_i. The latter terms of the decomposition are the interactions. They give information about the combined influence of two or more inputs taken together. We will not consider them further in this paper.

Plotting the main effects, $z_i(v_i)$ for each i gives a visual impression of the relative importance of each input to the variation in the output. This visual impression is heightened if the inputs are normalized (to the range of 0–1, for example, for uniformly distributed inputs), allowing all the main effects to be plotted together on the same plot. See Section VI where we present main effects plots for the LCM RTM.

To compute the main effects requires the evaluation of a $(d-1)$-dimensional integral. For even moderately complex functions $f(v)$, it will be impossible to evaluate this integral analytically. Indeed, for most cases of interest, an analytic form for $f(v)$ does not exist, rather, $f(v)$ only exists as a computer program. In these cases, $z_i(v_i)$ must be computed numerically. If evaluating $f(v)$ for a given v requires appreciable computation, then the standard methods of numerical integration, multidimensional quadrature and Monte Carlo integration, will be too computationally intensive to be practical. It is therefore useful to approximate $f(v)$ in such a way that the integrals required can be evaluated analytically. This allows the straightforward computation of the main effects of the approximation and also the computation of the uncertainty introduced by the approximation to $f(v)$. This is given in Sections IV and V; in particular, the details of the GP approximation we use for $f(v)$

are provided in Section IV, and its application to computing the main effects and sensitivity indices is developed in Section V.

B. Sensitivity Indices

The sensitivity indices are based on the variances of the terms in the decomposition of $f(\boldsymbol{v})$ given in (1). Specifically, consider

$$V_i = \text{Var}\left\{E(Y|v_i)\right\} = E\left[(E(Y|v_i))^2\right] - (E(Y))^2.$$

This is the expected amount by which the uncertainty in y will be reduced if we learn the true value of v_i [22]. It thus gives a measure of how much of the variance of y is due to input v_i. The V_i's can be normalized to

$$S_i = V_i/\text{Var}(Y)$$

so that the sum of all the S_i's and higher order terms ($S_{i,j}$, $S_{i,j,k}$, etc.) is unity. Thus, the value of S_i gives the relative importance of input v_i. The S_i's can also be used to direct improvements—reducing the uncertainty on the input with the largest S_i will have the greatest effect in reducing the uncertainty of the model output. This can be used to direct data collection work.

Computing the V_i's and S_i's can be complex, even under the GP approximation to $f(\boldsymbol{v})$. See Section V for details.

IV. APPROXIMATING THE LCM USING A GP

As discussed in the previous section, computing the main effects and sensitivity indices requires evaluating multidimensional integrals over arguments that include the RTM response $f(\boldsymbol{v})$. There are two approaches available, either evaluating a numerical approximation of the integral itself or forming an approximation to the argument of the integral, where the approximation enables the integrals to be evaluated analytically. The choice between these two approaches depends on a number of factors. In terms of the required computation, the tradeoff is between the numerical evaluation of the integral (typically via Monte Carlo integration) and the computation required to estimate the parameters of the approximation.

Regarding the main effects, the direct numerical approximation of the integrals in (2) requires evaluations of $f(\boldsymbol{v})$ over a sufficiently dense grid in $\boldsymbol{v}$. It will thus typically be feasible under small to moderate dimensions for the input space and for computationally reasonable functions $f(\boldsymbol{v})$ (which is indeed the case for the LCM). However, even for computationally inexpensive models $f(\boldsymbol{v})$, the same approach for the sensitivity indices V_i becomes substantially more challenging to implement for moderate number of inputs and is, arguably, not viable for high-dimensional input spaces. This becomes clear by inspection of the integrals required for the evaluation of the $E[(E(Y|v_i))^2]$; see Appendices I and II. Hence, in general, for global sensitivity analysis there is clear utility in approximating the model function $f(\boldsymbol{v})$ even for computer models that are relatively inexpensive to evaluate. As a concrete example, in [35], the analysis of a 10-D fire-propagation model required 10^6 simulations to perform global sensitivity analysis. By contrast,

a GP emulator can be built using much fewer samples—only 250 were needed to emulate the LCM (see Section VI).

As importantly, looking beyond sensitivity analysis, the construction of a statistical model as an emulator for the model output $f(\boldsymbol{v})$ provides scope for different types of practically important probabilistic analyses of the computer model. This has been discussed briefly in Section I and is elaborated in Section VII.

The approximation that we use for the LCM is provided by a GP. GPs are probability distributions over *functions*. Rather than placing a distribution over a (small) set of parameters, a GP places a distribution directly over the function of interest. Under a GP probability model for function $f(\cdot)$, the joint distribution of $(f(\boldsymbol{v}_1), \ldots, f(\boldsymbol{v}_k))$ is multivariate Gaussian for any finite set of input points $\boldsymbol{v}_1, \ldots, \boldsymbol{v}_k$. It is this property that allows for tractable computation—whereas the GP is defined over an infinite dimensional quantity (the continuous function $f(\boldsymbol{v})$), any computation is necessarily done over only a finite set of locations.

A GP is specified by its mean function $E(f(\boldsymbol{v}))$ and its covariance function $\text{Cov}(f(\boldsymbol{v}), f(\boldsymbol{v}'))$. The flexibility of choosing and adapting the mean and covariance functions allows a GP model to be successfully used to approximate a wide spectrum of functions $f(\boldsymbol{v})$, based on a set of training examples, $\boldsymbol{d} = \{\boldsymbol{y}, \boldsymbol{x}_1, \ldots, \boldsymbol{x}_n\}$, where $\boldsymbol{y} = (y_1, \ldots, y_n)$ and y_i is the response $f(\boldsymbol{x}_i)$ at observed input point $\boldsymbol{x}_i$, $i = 1, \ldots, n$. The set of training examples is chosen carefully to optimally sample the input space. Here, we used a Latin Hypercube design [36] to choose the set of inputs to the LCM. The other choices made were to use a constant mean function $E(f(\boldsymbol{v})) = \mu$, a constant variance $\text{Var}(f(\boldsymbol{v})) = \sigma^2$, and the product Gaussian correlation function

$$\text{Corr}\left(f(\boldsymbol{v}), f(\boldsymbol{v}'); \boldsymbol{\theta}\right) = \exp\left(-\sum_{\ell=1}^{d} \frac{(v_\ell - v'_\ell)^2}{\gamma_\ell}\right)$$

where $\boldsymbol{\theta} = (\gamma_1, \ldots, \gamma_d)$ and d is the dimension of the input space. The γ parameters give a measure of the scale over which the function $f(\boldsymbol{v})$ varies in each input dimension, and σ^2, the variance of the GP, determines the overall scale of $f(\boldsymbol{v})$. Using these mean and correlation functions, the GP defines the joint distribution

$$p(\boldsymbol{y}|\boldsymbol{\theta}, \mu, \sigma^2) = \frac{1}{(2\pi\sigma^2)^{n/2}|C(\boldsymbol{\theta})|^{1/2}}$$
$$\times \exp\left(-\frac{1}{2\sigma^2}(\boldsymbol{y} - \mu\mathbf{1}_n)^T C^{-1}(\boldsymbol{\theta})(\boldsymbol{y} - \mu\mathbf{1}_n)\right) \quad (3)$$

where $C(\boldsymbol{\theta})$ is the correlation matrix with (i, j)th element $\text{Corr}(f(\boldsymbol{x}_i), f(\boldsymbol{x}_j); \boldsymbol{\theta})$ and $\mathbf{1}_n$ denotes an n-dimensional vector with all elements equal to one.

We use the set of training examples $\boldsymbol{d}$ to estimate the parameters $\{\boldsymbol{\theta}, \mu, \sigma^2\}$ of the GP model using maximum likelihood estimation. From (3), the log likelihood is

$$\mathcal{L} = -\frac{1}{2\sigma^2}(\boldsymbol{y} - \mu\mathbf{1}_n)^T C^{-1}(\boldsymbol{\theta})(\boldsymbol{y} - \mu\mathbf{1}_n)$$
$$-\frac{1}{2}\log|C(\boldsymbol{\theta})| - \frac{n}{2}\log(2\pi\sigma^2). \quad (4)$$

The derivatives of $\mathcal{L}$ with respect to each of the parameters can be straightforwardly derived [16]. Maximizing $\mathcal{L}$ results in a point estimate for the parameters, denoted by $\{\hat{\boldsymbol{\theta}}, \hat{\mu}, \hat{\sigma}^2\}$, that we use when evaluating the main effects. Note that using point estimates for these parameters will cause the uncertainty of the main effects to be underestimated. In future work, we will consider a fully inferential Bayesian approach where expectations are also taken with respect to these parameters.

Once the GP model parameters are estimated, the first quantities of interest are the predictive distributions for sets of new inputs, conditioned on the training examples. From the definition of the GP, these distributions will be Gaussian. For a single new input $\boldsymbol{v}$, the predictive distribution for $f(\boldsymbol{v})$ has mean

$$m \equiv m(\boldsymbol{v}; \hat{\mu}, \hat{\boldsymbol{\theta}}, \boldsymbol{d}) = \hat{\mu} + \boldsymbol{r}^T(\boldsymbol{v})C^{-1}(\boldsymbol{y} - \hat{\mu}\mathbf{1}_n)$$

and variance

$$S \equiv S(\boldsymbol{v}; \hat{\mu}, \hat{\sigma}^2, \hat{\boldsymbol{\theta}}, \boldsymbol{d}) = \hat{\sigma}^2 \left(1 - \boldsymbol{r}^T(\boldsymbol{v})C^{-1}\boldsymbol{r}(\boldsymbol{v})\right).$$

Here, $\boldsymbol{r}(\boldsymbol{v})$ is the $n \times 1$ vector with ith element given by $\mathrm{Corr}(f(\boldsymbol{v}), f(\boldsymbol{x}_i)) = \exp(-\sum_{\ell=1}^{d}(v_\ell - x_{i\ell})^2/\hat{\gamma}_\ell)$, and $C \equiv C(\hat{\boldsymbol{\theta}})$ is the observed $n \times n$ correlation matrix with (i, j)th element given by $\exp(-\sum_{\ell=1}^{d}(x_{i\ell} - x_{j\ell})^2/\hat{\gamma}_\ell)$. Recall that the $\boldsymbol{x}_i$'s are the input values of the training examples.

The joint predictive distribution for $(f(\boldsymbol{v}), f(\boldsymbol{v}'))$ corresponding to generic inputs $\boldsymbol{v} = (v_1, \ldots, v_d)$ and $\boldsymbol{v}' = (v_1', \ldots, v_d')$ is bivariate normal with (2×1) mean vector

$$\boldsymbol{w} = \hat{\mu}\mathbf{1}_2 + R^T(\boldsymbol{v}, \boldsymbol{v}')C^{-1}(\boldsymbol{y} - \hat{\mu}\mathbf{1}_n) \tag{5}$$

and (2×2) covariance matrix

$$W = \hat{\sigma}^2 \left(B(\boldsymbol{v}, \boldsymbol{v}') - R^T(\boldsymbol{v}, \boldsymbol{v}')C^{-1}R(\boldsymbol{v}, \boldsymbol{v}')\right) \tag{6}$$

where $B(\boldsymbol{v}, \boldsymbol{v}')$ is the (2×2) observed correlation matrix for $(f(\boldsymbol{v}), f(\boldsymbol{v}'))$ with off-diagonal element given by $\exp(-\sum_{\ell=1}^{d}(v_\ell - v_\ell')^2/\hat{\gamma}_\ell)$, and $R(\boldsymbol{v}, \boldsymbol{v}')$ is the $(n \times 2)$ matrix with first-column elements $\exp(-\sum_{\ell=1}^{d}(v_\ell - x_{i\ell})^2/\hat{\gamma}_\ell)$, $i = 1, \ldots, n$, and analogously for the second-column elements replacing v_ℓ with v_ℓ'.

V. APPROXIMATING THE MAIN EFFECTS AND SENSITIVITY INDICES USING THE GP APPROXIMATION TO THE LCM

Computing the main effects requires the evaluation of $E(Y|v_j)$, for $j = 1, \ldots, d$, and $E(Y)$, as indicated in (2). However, we recall that we are approximating the function $y = f(\boldsymbol{v})$ by a GP model, and we must account for this approximation by computing $E^*\{E(Y|v_j)\}$ and $E^*\{E(Y)\}$, where we use $E^*\{\}$, $\mathrm{Var}^*\{\}$, and $\mathrm{Cov}^*\{\}$ to indicate expectation, variance, and covariance, respectively, with respect to the GP predictive distributions. We give details of these quantities here.

For the global mean, we have

$$E(Y) = \int_{\boldsymbol{v}} f(\boldsymbol{v}) \prod_{\ell=1}^{d} dH_\ell(v_\ell)$$

where $H(\boldsymbol{v}) = \prod_{\ell=1}^{d} H_\ell(v_\ell)$ is the input distribution, comprising independent components $H_\ell(v_\ell)$, which are uniform distributions over ranges (a_ℓ, b_ℓ), $\ell = 1, \ldots, d$. Therefore

$$E^*\{E(Y)\} = \int E(Y)dN(f(\boldsymbol{v}); m, S)$$

$$= \int_{\boldsymbol{v}} m(\boldsymbol{v}) \prod_{\ell=1}^{d} dH_\ell(v_\ell)$$

$$= \int_{\boldsymbol{v}} \left\{\hat{\mu} + \boldsymbol{r}^T(\boldsymbol{v})C^{-1}(\boldsymbol{y} - \hat{\mu}\mathbf{1}_n)\right\} \prod_{\ell=1}^{d} dH_\ell(v_\ell)$$

$$= \hat{\mu} + \boldsymbol{T}^T C^{-1}(\boldsymbol{y} - \hat{\mu}\mathbf{1}_n) \tag{7}$$

where $\boldsymbol{T}$ is the $n \times 1$ vector with ith element given by

$$\prod_{\ell=1}^{d} \left\{\int_{a_\ell}^{b_\ell} \exp(-(v_\ell - x_{i\ell})^2/\hat{\gamma}_\ell)(b_\ell - a_\ell)^{-1}dv_\ell\right\}.$$

Regarding the conditional expectation $E(Y|v_j)$, for each value u_j of the jth input, we have

$$E(Y|u_j) = \int_{\{v_\ell:\ell \neq j\}} f(v_1, \ldots, u_j, \ldots, v_d) \prod_{\{\ell:\ell \neq j\}} dH_\ell(v_\ell)$$

and thus

$$E^*\{E(Y|u_j)\}$$

$$= \int E(Y|u_j)dN\left(f(v_1, \ldots, u_j, \ldots, v_d); m, S\right)$$

$$= \int_{\{v_\ell:\ell \neq j\}} m(v_1, \ldots, u_j, \ldots, v_d) \prod_{\{\ell:\ell \neq j\}} dH_\ell(v_\ell)$$

$$= \hat{\mu} + \boldsymbol{T}_j^T(u_j)C^{-1}(\boldsymbol{y} - \hat{\mu}\mathbf{1}_n) \tag{8}$$

where $\boldsymbol{T}_j(u_j)$ is the $(n \times 1)$ vector with ith element given by the following:

$$\exp\left(-\frac{(u_j - x_{ij})^2}{\hat{\gamma}_j}\right)$$

$$\times \prod_{\{\ell:\ell \neq j\}} \left\{\int_{a_\ell}^{b_\ell} \exp\left(-\frac{(v_\ell - x_{i\ell})^2}{\hat{\gamma}_\ell}\right) \frac{1}{b_\ell - a_\ell}dv_\ell\right\}. \tag{9}$$

The previous expressions provide point estimates for all main effects associated with the d inputs. In particular, for each input $j = 1, \ldots, d$, $E^*\{E(Y|u_j)\}$ can be computed over a grid of u_j values to obtain point estimates for the functions $E(Y|u_j)$ (or for $E(Y|u_j) - E(Y)$ using also $E^*\{E(Y)\}$). These estimates can be compared graphically (linear transformations can be applied so that all inputs are on the same scale).

For a measure of the uncertainty associated with these estimates, we use

$$\mathrm{Var}^*\{E(Y|u_j)\} = E^*\left\{(E(Y|u_j))^2\right\} - (E^*\{E(Y|u_j)\})^2.$$

TABLE II
WAVELENGTH FOR EACH BAND USED AND THE
CORRESPONDING MODIS BAND NUMBER

band number	wavelength (nm)	MODIS band
1	469	ref3
2	555	ref4
3	1240	ref5
4	1640	ref6
5	2130	ref7
6	667	ref13
7	748	ref15
8	870	ref16

Because we already have the expression for $E^*\{E(Y|u_j)\}$ from the previous derivation, what is needed is an expression for $E^*\{(E(Y|u_j))^2\}$. This derivation is given in Appendix I, resulting in

$$\text{Var}^*\{E(Y|u_j)\} = \hat{\sigma}^2\left(e - \boldsymbol{T}_j^T(u_j)C^{-1}\boldsymbol{T}_j(u_j)\right)$$

where e is given by (15) of Appendix I.

The sensitivity indices are defined by

$$S_j = \frac{\text{Var}(E(Y|u_j))}{\text{Var}(Y)}, \qquad j = 1, \ldots, d.$$

Computing $E^*\{S_j\}$ cannot be done analytically, even under the GP approximation; therefore, we approximate it by computing the ratio of $E^*\{\text{Var}(E(Y|u_j))\}$ and $E^*\{\text{Var}(Y)\}$. (In future work, we will use a Bayesian approach implemented via Markov chain Monte Carlo (MCMC) methods [37] to estimate the entire distribution of S_j under the GP approximation, allowing the uncertainty of the sensitivity indices to also be determined.) We have

$$E^*\{\text{Var}(E(Y|u_j))\} = E^*\left\{E\left[(E(Y|u_j))^2\right]\right\} - E^*\left\{(E(Y))^2\right\}$$

$$E^*\{\text{Var}(Y)\} = E^*\{E(Y^2)\} - E^*\{(E(Y))^2\}.$$

The expressions for these terms are not difficult to derive, although care is needed. They are given in Appendix II.

VI. RESULTS

The proposed methodology has been applied to execute a global sensitivity analysis and to analyze both the sensitivity of the spectral hemispherical reflectance to the defined input parameters and the relative contribution of each of the parameters to the model output.

To obtain the training data for the GP model, we generated a 250-point Latin Hypercube design over the 7-D space of inputs given in Table I. The LAD variable was set to planophile (leaves mostly horizontal), and the sun angle was set to zenith. Although the sun angle will vary, for any given satellite scene, it will be known, and therefore, we do not consider it as one of the inputs for this analysis. The LAD will be determined largely by knowledge of the biome of the area being observed. The LCM was run at eight wavelengths, given in Table II, corresponding to eight of the MODIS bands that are sensitive to vegetation. The corresponding MODIS band is also given in Table II. Note

that the bands are in MODIS band order, not in wavelength order.

Fig. 2 shows the plots of the main effects for the seven input variables for each of the eight bands. The larger the variation of the main effect plot, the greater the influence of that input on the LCM response. To display the main effects for all parameters on a single plot, the range of each input (given in Table I) has been normalized to 0–1. The slope of each main effect plot gives information as to whether the output is an increasing or decreasing function of that input. The relative scale of the main effects can be easily compared visually. The absolute scale depends on the absolute magnitude of the model output. Fig. 3 shows the main effects for band 4 and includes the uncertainty bounds due to approximating the LCM by the GP. The uncertainties are extremely small.

To correctly interpret the results and to put them in the right perspective, we divide the input parameters in two categories, i.e., absorption and scattering driven. Biochemical inputs, i.e., chlorophyll, water, lignin, and protein are absorption driven because their effect heavily depends on wavelength, and they mainly affect the absorption characteristic of vegetation canopies [25]. Conversely, LAI, leaf thickness, and soil brightness can be categorized as scattering driven because they directly influence the transport of photons in the medium. The main effects and sensitivity indices are analyzed next.

The LCM is most sensitive to LAI in the near-infrared (NIR) region of the spectrum (bands 7 and 8). It is shown in Fig. 2 that the LAI effect is highly nonlinear, and the behavior is such that, in bands 7, 8, and 3, an increase in LAI produces an increase in reflectance. Conversely, the effect is opposite in the visible, i.e., increases in LAI produce a decrease in the hemispherical reflectance. This trend is known. [38], [39]. The sensitivity indices (Table III) show that LAI is the major contributor in the bands which are most sensitive.

Chlorophyll, on the other hand, is expected to be extremely influential in the visible—it is the prevailing factor that dominates the reflectance. Its effect is strong in the visible (bands 1, 2, and 6), whereas it dramatically decreases at the red edge (band 7) to eventually disappear in the rest of the spectrum. The decrease of sensitivity to chlorophyll at the red edge is only found because the MODIS bands do not cover the actual red edge which is located around 730 nm. Conversely, chlorophyll does not absorb light after 760 nm. As shown in Fig. 3, band 4 shows basically no sensitivity for chlorophyll with small quantified uncertainty in the result.

Water contribution occurs mainly in the short-wave infrared because it exhibits higher absorption which peaks around 1445 and 1950 nm. Indeed, water is ranked as the second and third major contributor to the reflectance in bands 5 and 4, respectively. Nevertheless, such bands are outside the atmospheric window. Conversely, the reflectance is weakly sensitive in the visible.

Protein is shown to be insensitive to most of the spectrum. Its effect as well as contribution are extremely small and can be only detected with difficulties in the NIR (e.g., band 8).

Lignin is one of the major surprising results. It is extremely sensitive in the short-wave infrared (bands 4 and 5) where it is also the major contributor to the hemispherical reflectance.
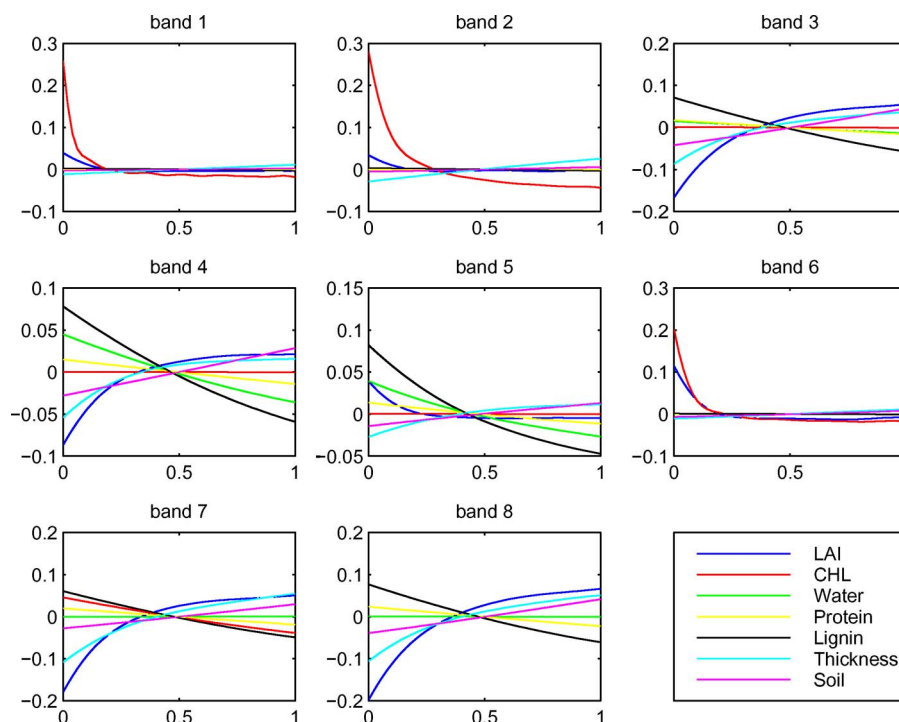
Fig. 2. Main effects for the LCM RTM.
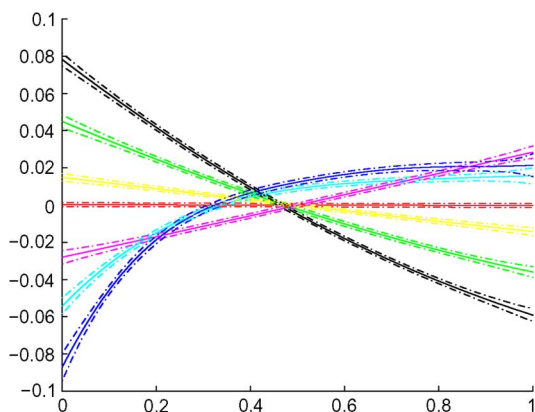
Fig. 3. Uncertainty in the main effects due to using the GP approximation to the LCM RTM. Band 4. Line colors as in Fig. 2.

TABLE III
SENSITIVITY INDICES FOR EACH INPUT FOR EACH SPECTRAL BAND

	band; wavelength (nm)							
	1	2	3	4	5	6	7	8
input	469	555	1240	1640	2130	667	748	870
LAI	0.05	0.01	0.43	0.16	0.04	0.28	0.41	0.48
CHL	0.80	0.83	0.00	0.00	0.00	0.56	0.08	0.00
Water	0.00	0.00	0.01	0.12	0.14	0.00	0.00	0.00
Protein	0.00	0.00	0.01	0.02	0.02	0.00	0.02	0.02
Lignin	0.00	0.00	0.19	0.36	0.53	0.00	0.13	0.16
Thick.	0.02	0.05	0.14	0.07	0.05	0.02	0.24	0.18
Soil	0.00	0.00	0.08	0.06	0.03	0.01	0.03	0.06
Total	0.88	0.90	0.86	0.80	0.81	0.87	0.90	0.90

This is mainly due to the strong absorption features in this part of the spectrum where the lignin absorption coefficient features a peak around 2110 nm.

Leaf thickness demonstrates a true scattering effect, and its response shows interesting features. It is mainly sensitive and has the major contribution in bands 3, 7, and 8. We believe that what we are seeing is that changing the leaf thickness has more influence on scattering than on absorption. Specifically, as we change the leaf thickness, the model assumes that the leaf mass is unchanged, meaning that the absorption has little effect as can be seen specifically in the NIR part of the spectrum.

The soil brightness has generally little effect. The spectrum for a typical soil was spectrally defined, and the brightness parameter is responsible for increasing the soil hemispherical reflectance, therefore simulating the dry–wet effect.

That the sensitivity indices do not sum to one indicates that interaction effects between two or more inputs are important in some bands, particularly bands 4 and 5. In future work, we will compute the second-order sensitivity indices that quantify which interactions are important.

The results described so far are for planophile LAD. We performed the same analysis for the other LAD values, namely, erectophile, extremophile, and plagiophile. The results for the main effects were largely similar, with the main effect for LAI being less pronounced for erectophile compared to planophile in bands 4 and 5 and thickness showing less effect in band 7. That the effect of changing LAD is apparent in the scattering variables is to be expected.

Tables IV and V show the sensitivity indices for LAI and thickness for the four LAD values. It is seen that the thickness input has a larger effect for planophile LAD (particularly in bands 7 and 8). Variation is seen for LAI when comparing erectophile LAD to the other values.

TABLE IV
SENSITIVITY INDICES FOR LAI FOR THE FOUR LAD VALUES.
(PLANOPHILE, ERECTOPHILE, EXTREMOPHILE, AND PLAGIOPHILE)

	band; wavelength (nm)							
	1	2	3	4	5	6	7	8
LAD	469	555	1240	1640	2130	667	748	870
Plan.	0.05	0.01	0.43	0.16	0.04	0.28	0.41	0.48
Erect.	0.14	0.06	0.32	0.05	0.16	0.45	0.37	0.42
Extr.	0.08	0.03	0.40	0.12	0.09	0.36	0.40	0.47
Plag.	0.07	0.02	0.43	0.15	0.06	0.32	0.43	0.50

TABLE V
SENSITIVITY INDICES FOR THICKNESS FOR THE FOUR LAD VALUES

	band; wavelength (nm)							
	1	2	3	4	5	6	7	8
Thick.	469	555	1240	1640	2130	667	748	870
Plan.	0.02	0.05	0.14	0.07	0.05	0.02	0.24	0.18
Erect.	0.01	0.02	0.02	0.00	0.00	0.00	0.08	0.05
Extr.	0.02	0.04	0.08	0.02	0.02	0.01	0.18	0.12
Plag.	0.01	0.03	0.07	0.01	0.01	0.01	0.15	0.11

Our results are consistent with, and extend, previous statistically based work. For example, [12] presented a methodology for sensitivity analysis based on the design of numerical experiments aimed at providing a comparison between four canopy RTMs coupled with a leaf-based RTM (PROSPECT, [29]). Their results are consistent with ours regarding LAI, chlorophyll, and soil brightness sensitivity behavior. That the response in bands 1, 2, and 6 is dominated by LAI and chlorophyll is consistent with the results of a much more restricted sensitivity analysis in [40].

These results show that analyzing the uncertainty characteristics of RTMs used in remote sensed data product generation is practical and important. It gives information on the level of accuracy needed in the model's inputs, can guide data collection efforts to most effectively reduce the uncertainties, and can guide further development effort for the RTMs themselves. It also gives information as to which of the model's inputs affect the output and, hence, which inputs it may be possible to determine from remotely sensed observations.

VII. FUTURE WORK

In this paper, we have developed a statistical framework for global sensitivity analysis in RTMs. In doing so, we have introduced tools that have much wider applicability than the sensitivity analyses presented here. In particular, the GP emulator approach can be used to address important problems in model calibration, validation, and inversion.

The remote sensing community spends much effort in collecting field data [41], [42] to calibrate and validate models—to determine how well a model matches reality and to inform model improvements. Using the GP emulator approach, we can model the field data as

$$\tilde{y}_j = f(\tilde{\boldsymbol{v}}_j) + b(\tilde{\boldsymbol{v}}_j) + \epsilon_j \qquad (10)$$

where $\tilde{y}_j$ are the observed field data corresponding to parameter values $\tilde{\boldsymbol{v}}_j$ and the ϵ_j's are measurement errors, for example, independent from an $N(0, \sigma_\epsilon^2)$ distribution. The response is composed of two terms, $f(\cdot)$, the GP model based on training

data, as described in Section IV, and $b(\cdot)$, a *bias* term, a second GP which models the difference between the model approximation and the measured field data. (In practice, $f(\cdot)$ and $b(\cdot)$ are learned simultaneously based on a likelihood function that comprises both RTM training data and field data.)

The resulting inference for $b(\cdot)$ for different regions of the input space can quantify the local performance of the model.

The determination of a calibrated, validated model incorporating the bias term allows a statistical inversion of the model to be performed, which respects the field data. In the usual manner, the error between the predictions and the satellite observations in a number of bands are taken to have a multivariate normal distribution. The inversion is regularized by the inclusion of a prior over LAI, which may depend on spatial position and biome type. Using the modeling framework in (10), the tools of statistical inference can be used to estimate the model inverse and its uncertainties.

The work outlined in this section is in progress and will be reported when appropriate.

APPENDIX I
VARIANCE OF THE MAIN EFFECTS

We give here the derivation of $E^*\{(E(Y|u_j))^2\}$ required in the expression for $\mathrm{Var}^*\{E(Y|u_j)\}$, which provides a measure of the uncertainty associated with the estimates of the main effects.

Note that

$$(E(Y|u_j))^2 = \left(\int\limits_{\{v_\ell : \ell \neq j\}} f(v_1, \ldots, u_j, \ldots, v_d) \prod_{\{\ell : \ell \neq j\}} dH_\ell(v_\ell) \right)^2$$

$$= \iint\limits_{\substack{\{v_\ell : \ell \neq j\} \\ \{v'_\ell : \ell \neq j\}}} f(v_1, \ldots, u_j, \ldots, v_d) f(v'_1, \ldots, u_j, \ldots, v'_d)$$

$$\times \prod_{\{\ell : \ell \neq j\}} dH_\ell(v_\ell) \prod_{\{\ell : \ell \neq j\}} dH_\ell(v'_\ell)$$

and thus, we need to take $E^*\{\cdot\}$ with respect to the GP-based bivariate predictive distribution for $(f(v_1, \ldots, u_j, \ldots, v_d), f(v'_1, \ldots, u_j, \ldots, v'_d))$. Specifically

$$E^*\left\{(E(Y|u_j))^2\right\} = \iint\limits_{\substack{\{v_\ell : \ell \neq j\} \\ \{v'_\ell : \ell \neq j\}}} E^*\{f(v_1, \ldots, u_j, \ldots, v_d)$$

$$\times f(v'_1, \ldots, u_j, \ldots, v'_d)\} \prod_{\{\ell : \ell \neq j\}} dH_\ell(v_\ell) \prod_{\{\ell : \ell \neq j\}} dH_\ell(v'_\ell) \quad (11)$$

where, using the standard covariance identity

$$E^*\{f(v_1, \ldots, u_j, \ldots, v_d) f(v'_1, \ldots, u_j, \ldots, v'_d)\}$$

$$= \mathrm{Cov}^*\{f(v_1, \ldots, u_j, \ldots, v_d), f(v'_1, \ldots, u_j, \ldots, v'_d)\}$$

$$+ (E^*\{f(v_1, \ldots, u_j, \ldots, v_d)\} E^*\{f(v'_1, \ldots, u_j, \ldots, v'_d)\}).$$

$$(12)$$

Denote by $\boldsymbol{R}_1 \equiv \boldsymbol{R}_1(v_1, \ldots, u_j, \ldots, v_d)$ and $\boldsymbol{R}_2 \equiv \boldsymbol{R}_2(v'_1, \ldots, u_j, \ldots, v'_d)$ the first and second columns, respectively, of the $(n \times 2)$ matrix $R(\boldsymbol{v}, \boldsymbol{v}')$ defined in Section IV. Note that, here, the input vectors we are working with, $(v_1, \ldots, u_j, \ldots, v_d)$ and $(v'_1, \ldots, u_j, \ldots, v'_d)$, have a common element u_j. Therefore, $\boldsymbol{R}_1$ is the $(n \times 1)$ vector with elements

$$\exp\left(-\frac{(u_j - x_{ij})^2}{\hat{\gamma}_j} - \sum_{\{\ell:\ell \neq j\}} \frac{(v_\ell - x_{i\ell})^2}{\hat{\gamma}_\ell}\right), \qquad i = 1, \ldots, n$$

and analogously for $\boldsymbol{R}_2$, replacing v_ℓ with v'_ℓ. Then, using (5) and (6), we obtain

$$E^* \{f(v_1, \ldots, u_j, \ldots, v_d)\} = \hat{\mu} + \boldsymbol{R}_1^T C^{-1}(\boldsymbol{y} - \hat{\mu}\boldsymbol{1}_n)$$

$$E^* \{f(v'_1, \ldots, u_j, \ldots, v'_d)\} = \hat{\mu} + \boldsymbol{R}_2^T C^{-1}(\boldsymbol{y} - \hat{\mu}\boldsymbol{1}_n)$$

$$\mathrm{Cov}^* \{f(v_1, \ldots, u_j, \ldots, v_d), f(v'_1, \ldots, u_j, \ldots, v'_d)\}$$

$$= \hat{\sigma}^2 \left\{\exp\left(-\sum_{\{\ell:\ell \neq j\}} \frac{(v_\ell - v'_\ell)^2}{\hat{\gamma}_\ell}\right) - \boldsymbol{R}_1^T C^{-1} \boldsymbol{R}_2\right\}. \quad (13)$$

Finally, substituting (12) and (13) in (11), we obtain for each $j = 1, \ldots, d$

$$E^* \left\{(E(Y|u_j))^2\right\} = \hat{\sigma}^2 \left(e - \boldsymbol{T}_j^T(u_j) C^{-1} \boldsymbol{T}_j(u_j)\right)$$

$$+ \left(\hat{\mu} + \boldsymbol{T}_j^T(u_j) C^{-1}(\boldsymbol{y} - \hat{\mu}\boldsymbol{1}_n)\right)^2 \quad (14)$$

where $\boldsymbol{T}_j(u_j)$ is the $(n \times 1)$ vector with the elements given in (9) of Section V, and

$$e = \prod_{\{\ell:\ell \neq j\}} \left\{\int_{a_\ell}^{b_\ell} \int_{a_\ell}^{b_\ell} \exp\left(-\frac{(v_\ell - v'_\ell)^2}{\hat{\gamma}_\ell}\right) \frac{dv_\ell dv'_\ell}{(b_\ell - a_\ell)^2}\right\}. \quad (15)$$

Note that the second term in (14) is $(E^*\{E(Y|u_j)\})^2$, and therefore, the required variance has the simpler expression

$$\mathrm{Var}^* \{E(Y|u_j)\} = \hat{\sigma}^2 \left(e - \boldsymbol{T}_j^T(u_j) C^{-1} \boldsymbol{T}_j(u_j)\right).$$

APPENDIX II
SENSITIVITY INDICES

Here, we present the details for computing the estimates of the first-order sensitivity indices $S_j = \mathrm{Var}(E(Y|u_j))/\mathrm{Var}(Y)$, which provide a measure of the portion of variability in the response due to the main effect for each input. As discussed in Section V, our estimates for the S_j, $j = 1, \ldots, d$, are based on $E^*\{\mathrm{Var}(E(Y|u_j))\}$ and $E^*\{\mathrm{Var}(Y)\}$. Regarding the estimate for the unconditional variance, we can write

$$E^* \{\mathrm{Var}(Y)\} = E^* \left\{E(Y^2)\right\} - E^* \left\{(E(Y))^2\right\}.$$

For the first term, we have

$$E^* \{E(Y^2)\} = E^* \left\{\int_{\boldsymbol{v}} f^2(\boldsymbol{v}) \prod_{\ell=1}^{d} dH_\ell(v_\ell)\right\}$$

$$= \int_{\boldsymbol{v}} E^* \{f^2(\boldsymbol{v})\} \prod_{\ell=1}^{d} dH_\ell(v_\ell)$$

$$= \int_{\boldsymbol{v}} (S + m^2) \prod_{\ell=1}^{d} dH_\ell(v_\ell)$$

where m and S are the mean and variance, respectively, of the predictive distribution for $f(\boldsymbol{v})$ given in Section IV. Substituting their expressions to the aforementioned equation, we obtain

$$E^* \{E(Y^2)\} = \hat{\sigma}^2 \int_{\boldsymbol{v}} \left(1 - \boldsymbol{r}^T(\boldsymbol{v}) C^{-1} \boldsymbol{r}(\boldsymbol{v})\right) \prod_{\ell=1}^{d} dH_\ell(v_\ell)$$

$$+ \int_{\boldsymbol{v}} \left\{\hat{\mu}^2 + 2\hat{\mu}\boldsymbol{r}^T(\boldsymbol{v}) C^{-1}(\boldsymbol{y} - \hat{\mu}\boldsymbol{1}_n)\right.$$

$$\left. + (\boldsymbol{r}^T(\boldsymbol{v}) C^{-1}(\boldsymbol{y} - \hat{\mu}\boldsymbol{1}_n))^2\right\} \prod_{\ell=1}^{d} dH_\ell(v_\ell)$$

$$= \hat{\sigma}^2 - \hat{\sigma}^2 \left(\int_{\boldsymbol{v}} \boldsymbol{r}^T(\boldsymbol{v}) C^{-1} \boldsymbol{r}(\boldsymbol{v}) \prod_{\ell=1}^{d} dH_\ell(v_\ell)\right)$$

$$+ \hat{\mu}^2 + 2\hat{\mu}\boldsymbol{T}^T C^{-1}(\boldsymbol{y} - \hat{\mu}\boldsymbol{1}_n)$$

$$+ \left(\int_{\boldsymbol{v}} (\boldsymbol{r}^T(\boldsymbol{v}) C^{-1}(\boldsymbol{y} - \hat{\mu}\boldsymbol{1}_n))^2 \prod_{\ell=1}^{d} dH_\ell(v_\ell)\right)$$

where $\boldsymbol{T}$ is the $n \times 1$ vector defined in Section V in the expression for $E^*\{E(Y)\}$ after (7). Regarding the two integrals in the equation, if we expand the quadratic form $\boldsymbol{r}^T(\boldsymbol{v}) C^{-1} \boldsymbol{r}(\boldsymbol{v})$ and apply the integral, we obtain

$$\int_{\boldsymbol{v}} \boldsymbol{r}^T(\boldsymbol{v}) C^{-1} \boldsymbol{r}(\boldsymbol{v}) \prod_{\ell=1}^{d} dH_\ell(v_\ell) = \sum_{i=1}^{n} \sum_{j=1}^{n} c_{ij} q_{ij}$$

where c_{ij} is the (i, j)th element of matrix C^{-1}, and

$$q_{ij} = \prod_{\ell=1}^{d} \left\{\int_{a_\ell}^{b_\ell} \exp\left(-\frac{(v_\ell - x_{i\ell})^2 + (v_\ell - x_{j\ell})^2}{\hat{\gamma}_\ell}\right) \frac{1}{b_\ell - a_\ell} dv_\ell\right\},$$

$$i, j = 1, \ldots, n.$$

(The q_{ij}'s are symmetric in (i, j).) Analogously, expanding the square $(\boldsymbol{r}^T(\boldsymbol{v}) C^{-1}(\boldsymbol{y} - \hat{\mu}\boldsymbol{1}_n))^2$ and taking the integral, we get

$$\int_{\boldsymbol{v}} (\boldsymbol{r}^T(\boldsymbol{v}) C^{-1}(\boldsymbol{y} - \hat{\mu}\boldsymbol{1}_n))^2 \prod_{\ell=1}^{d} dH_\ell(v_\ell)$$

$$= \sum_{i=1}^{n} z_i^2 q_{ii} + 2 \sum_{i=1}^{n} \sum_{j=i+1}^{n} z_i z_j q_{ij}$$

where z_i denotes the ith element of the $n \times 1$ vector $C^{-1}(\boldsymbol{y} - \hat{\mu}\boldsymbol{1}_n)$.

For the second term, we can write

$$E^* \left\{ (E(Y))^2 \right\}$$

$$= E^* \left\{ \left(\int_{\boldsymbol{v}} f(\boldsymbol{v}) \prod_{\ell=1}^{d} dH_\ell(v_\ell) \right)^2 \right\}$$

$$= E^* \left\{ \int_{\boldsymbol{v}} \int_{\boldsymbol{v}'} f(\boldsymbol{v}) f(\boldsymbol{v}') \prod_{\ell=1}^{d} dH_\ell(v_\ell) \prod_{\ell=1}^{d} dH_\ell(v'_\ell) \right\}$$

$$= \int_{\boldsymbol{v}} \int_{\boldsymbol{v}'} E^* \left\{ f(\boldsymbol{v}) f(\boldsymbol{v}') \right\} \prod_{\ell=1}^{d} dH_\ell(v_\ell) \prod_{\ell=1}^{d} dH_\ell(v'_\ell)$$

and thus, $E^*\{(E(Y))^2\}$ can be expressed as

$$\int_{\boldsymbol{v}} \int_{\boldsymbol{v}'} \text{Cov}^* \left\{ f(\boldsymbol{v}), f(\boldsymbol{v}') \right\} \prod_{\ell=1}^{d} dH_\ell(v_\ell) \prod_{\ell=1}^{d} dH_\ell(v'_\ell)$$

$$+ \int_{\boldsymbol{v}} \int_{\boldsymbol{v}'} \left\{ E^*(f(\boldsymbol{v})) \, E^* (f(\boldsymbol{v}')) \right\} \prod_{\ell=1}^{d} dH_\ell(v_\ell) \prod_{\ell=1}^{d} dH_\ell(v'_\ell). \quad (16)$$

Let $\boldsymbol{r}'(\boldsymbol{v}')$ denote the $(n \times 1)$ vector with ith element given by $\exp(-\sum_{\ell=1}^{d}(v'_\ell - x_{i\ell})^2/\hat{\gamma}_\ell)$. Then, analogously to the expressions in (13), we have

$$E^* \{f(\boldsymbol{v})\} = \hat{\mu} + \boldsymbol{r}^T(\boldsymbol{v}) C^{-1}(\boldsymbol{y} - \hat{\mu}\boldsymbol{1}_n)$$

$$E^* \{f(\boldsymbol{v}')\} = \hat{\mu} + \boldsymbol{r}'^T(\boldsymbol{v}') C^{-1}(\boldsymbol{y} - \hat{\mu}\boldsymbol{1}_n)$$

$$\text{Cov}^* \{f(\boldsymbol{v}), f(\boldsymbol{v}')\} = \hat{\sigma}^2 \left\{ \exp\left(-\sum_{\ell=1}^{d} \frac{(v_\ell - v'_\ell)^2}{\hat{\gamma}_\ell} \right) \right.$$

$$\left. - \boldsymbol{r}^T(\boldsymbol{v}) C^{-1} \boldsymbol{r}'(\boldsymbol{v}') \right\}. \quad (17)$$

Therefore, substituting (17) in (16) and applying the integrations, we finally obtain

$$E^* \left\{ (E(Y))^2 \right\} = \hat{\sigma}^2 (e^* - \boldsymbol{T}^T C^{-1} \boldsymbol{T})$$

$$+ \left(\hat{\mu} + \boldsymbol{T}^T C^{-1}(\boldsymbol{y} - \hat{\mu}\boldsymbol{1}_n) \right)^2$$

where

$$e^* = \prod_{\ell=1}^{d} \left\{ \int_{a_\ell}^{b_\ell} \int_{a_\ell}^{b_\ell} \exp\left(-\frac{(v_\ell - v'_\ell)^2}{\hat{\gamma}_\ell} \right) \frac{1}{(b_\ell - a_\ell)^2} dv_\ell dv'_\ell \right\}$$

and, again, $\boldsymbol{T}$ is the $(n \times 1)$ vector given after (7) in Section V.

Turning to the estimate for $\text{Var}(E(Y|u_j))$, we have

$$E^* \{\text{Var}(E(Y|u_j))\} = E^* \left\{ E \left[(E(Y|u_j))^2 \right] \right\} - E^* \left\{ (E(Y))^2 \right\}$$

and therefore, we only need the expression for $E^*\{E[(E(Y|u_j))^2]\}$. In particular

$$E^* \left\{ E \left[(E(Y|u_j))^2 \right] \right\}$$

$$= E^* \left\{ \int (E(Y|u_j))^2 \, dH_j(u_j) \right\}$$

$$= \int E^* \left\{ (E(Y|u_j))^2 \right\} dH_j(u_j)$$

$$= \int \hat{\sigma}^2 \left(e - \boldsymbol{T}_j^T(u_j) C^{-1} \boldsymbol{T}_j(u_j) \right)$$

$$+ \left(\hat{\mu} + \boldsymbol{T}_j^T(u_j) C^{-1}(\boldsymbol{y} - \hat{\mu}\boldsymbol{1}_n) \right)^2 dH_j(u_j)$$

$$= \hat{\sigma}^2 e - \hat{\sigma}^2 \left\{ \int \boldsymbol{T}_j^T(u_j) C^{-1} \boldsymbol{T}_j(u_j) dH_j(u_j) \right\}$$

$$+ \hat{\mu}^2 + 2\hat{\mu} \boldsymbol{T}^T C^{-1}(\boldsymbol{y} - \hat{\mu}\boldsymbol{1}_n)$$

$$+ \left\{ \int \left(\boldsymbol{T}_j^T(u_j) C^{-1}(\boldsymbol{y} - \hat{\mu}\boldsymbol{1}_n) \right)^2 dH_j(u_j) \right\}.$$

The two integrals in the equation can be computed as follows. First

$$\int \boldsymbol{T}_j^T(u_j) C^{-1} \boldsymbol{T}_j(u_j) dH_j(u_j) = \sum_{m=1}^{n} \sum_{k=1}^{n} A_m A_k c_{mk} I_{km}$$

where

$$I_{km} = \int_{a_j}^{b_j} \exp\left(-\frac{(u_j - x_{mj})^2 + (u_j - x_{kj})^2}{\hat{\gamma}_j} \right) \frac{1}{b_j - a_j} du_j$$

and where, again, c_{mk} is the (m,k)th element of matrix C^{-1}, and

$$A_m = \prod_{\{\ell: \ell \neq j\}} \left\{ \int_{a_\ell}^{b_\ell} \exp\left(-\frac{(v_\ell - x_{m\ell})^2}{\hat{\gamma}_\ell} \right) \frac{1}{b_\ell - a_\ell} dv_\ell \right\},$$

$$m = 1, \ldots, n.$$

Moreover

$$\int \left(\boldsymbol{T}_j^T(u_j) C^{-1}(\boldsymbol{y} - \hat{\mu}\boldsymbol{1}_n) \right)^2 dH_j(u_j)$$

$$= \sum_{m=1}^{n} z_m^2 \left\{ A_m^2 \int_{a_j}^{b_j} \exp\left(-\frac{2(u_j - x_{mj})^2}{\hat{\gamma}_j} \right) \frac{1}{b_j - a_j} du_j \right\}$$

$$+ 2 \sum_{m=1}^{n} \sum_{k=m+1}^{n} z_m z_k A_m A_k I_{km}$$

where I_{km} is defined previously and z_m denotes the mth element of the vector $C^{-1}(\boldsymbol{y} - \hat{\mu}\boldsymbol{1}_n)$.

REFERENCES

[1] A. Huete and H. Liu, "An error and sensitivity analysis of the atmospheric- and soil-correcting variants of the NDVI for the MODIS-EOS," *IEEE Trans. Geosci. Remote Sens.*, vol. 32, no. 4, pp. 897–905, Jul. 1994.

[2] C. Justice, E. Vermote, J. Townshend, R. Defries, D. Roy, D. Hall, V. Salomonson, J. Privette, G. Riggs, A. Strahler, W. Lucht, R. Myneni, Y. Knyazikhin, S. Running, R. Nemani, Z. Wan, A. Huete, W. van Leeuwen, R. Wolfe, L. Giglio, J.-P. Muller, P. Lewis, and M. Barnsley, "The moderate resolution imaging spectroradiometer (MODIS): Land remote sensing for global change research," *IEEE Trans. Geosci. Remote Sens.*, vol. 36, no. 4, pp. 1228–1249, Jul. 1998.

[3] W. Barnes, T. Pagano, and V. Salomonson, "Prelaunch characteristics of the moderate resolution imaging spectroradiometer (MODIS) on EOS-AM1," *IEEE Trans. Geosci. Remote Sens.*, vol. 36, no. 4, pp. 1088–1100, Jul. 1998.

[4] S. Hook, G. Vaughan, H. Tonooka, and S. Schladow, "Absolute radiometric in-flight validation of mid infrared and thermal infrared data from ASTER and MODIS on the Terra spacecraft using the Lake Tahoe CA/NV, USA, automated validation site," *IEEE Trans. Geosci. Remote Sens.*, vol. 45, no. 6, pp. 1798–1807, Jun. 2007.

[5] X. Xiong, N. Che, and W. Barnes, "Terra MODIS on-orbit spectral characterization and performance," *IEEE Trans. Geosci. Remote Sens.*, vol. 44, no. 8, pp. 2198–2206, Aug. 2006.

[6] J. Morisette, F. Baret, and S. Liang, "Special issue on global land product validation," *IEEE Trans. Geosci. Remote Sens.*, vol. 44, no. 7, pp. 1695–1697, Jul. 2006.

[7] W. Yang, B. Tan, D. Huang, M. Rautiainen, N. Shabanov, Y. Wang, J. Privette, K. Huemmrich, R. Fenshold, I. Sandholt, M. Weiss, D. Ahl, S. Glower, R. Nemani, Y. Knyazikhin, and R. Myneni, "MODIS leaf area index products: From validation to algorithm improvement," *IEEE Trans. Geosci. Remote Sens.*, vol. 44, no. 7, pp. 1885–1989, Jul. 2006.

[8] B. Ganapol, L. Johnson, C. Hlavka, D. Peterson, and B. Bond, "LCM2: A coupled leaf/canopy radiative transfer model," *Remote Sens. Environ.*, vol. 70, no. 2, pp. 153–166, Nov. 1999.

[9] Y. Knyazikhin, J. Martonchik, R. Myneni, D. Diner, and S. Running, "Synergistic algorithm for estimating vegetation canopy leaf area index and fraction of absorbed photosynthetically active radiation from MODIS and MISR data," *J. Geophys. Res.*, vol. 103, no. D24, pp. 32 257–32 276, Jan. 1998.

[10] A. Saltelli, K. Chan, and E. Scott, *Sensitivity Analysis*. Chichester, U.K.: Wiley, 2000.

[11] A. Saltelli, "Sensitivity analysis: Could better methods be used?" *J. Geophys. Res.*, vol. 104, no. D3, pp. 3789–3793, Feb. 1999.

[12] C. Bacour, S. Jaquemoud, Y. Tourbier, M. Dechambre, and J.-P. Frangi, "Design and analysis of numerical experiments to compare four reflectance models," *Remote Sens. Environ.*, vol. 79, no. 1, pp. 72–83, Jan. 2002.

[13] R. Brun, P. Reichert, and H. Kuensch, "Practical identifiability analysis of large environmental simulation models," *Water Resources Res.*, vol. 37, no. 4, pp. 1015–1030, Apr. 2001.

[14] P. Bowyer, F. Danson, and N. Trodd, "Methods of sensitivity analysis in remote sensing: Implications for canopy reflectance model inversion," in *Proc. Int. Geosci. Remote Sens. Symp.*, Jul. 2003, vol. 6, pp. 3839–3841.

[15] D. Mackay, "Introduction to Gaussian process," *NATO ASI Ser. F: Comput. Syst. Sci.*, vol. 168, pp. 133–166, 1998.

[16] C. Rasmussen and C. Williams, *Gaussian Processes for Machine Learning*. Cambridge, MA: MIT Press, 2006.

[17] R. Neal, "Regression and classification using Gaussian process priors," in *Bayesian Statistics 6*, J. Bernardo, J. Berger, A. Dawid, and A. Smith, Eds. London, U.K.: Oxford Univ. Press, 1998, pp. 475–501.

[18] J. Sacks, W. Welch, W. Mitchell, and H. Wynn, "Design and analysis of computer experiments," *Stat. Sci.*, vol. 4, no. 4, pp. 409–435, Nov. 1989.

[19] C. Currin, T. Mitchell, M. Morris, and D. Ylvisaker, "Bayesian prediction of deterministic functions, with applications to the design and analysis of computer experiments," *J. Amer. Stat. Assoc.*, vol. 86, pp. 953–963, Dec. 1991.

[20] W. Welch, R. Buck, J. Sacks, H. Wynn, T. Mitchell, and M. Morris, "Screening, predicting and computer experiments," *Technometrics*, vol. 34, no. 1, pp. 15–25, Feb. 1992.

[21] T. Santner, B. Williams, and W. Notz, *The Design and Analysis of Computer Experiments*, Springer Series in Statistics. Berlin, Germany: Springer-Verlag, 2003.

[22] J. Oakley and A. O'Hagan, "Probabilistic sensitivity analysis of complex models: A Bayesian approach," *J. Roy. Stat. Soc., Ser. B. Stat. Methodol.*, vol. 66, no. 3, pp. 751–769, 2004.

[23] M. Kennedy and A. O'Hagan, "Bayesian calibration of computer models (with discussion)," *J. Roy. Stat. Soc., Ser. B. Stat. Methodol.*, vol. 63, no. 3, pp. 425–464, 2001.

[24] M. Bayarri, J. Berger, D. Higdon, M. Kennedy, A. Kottas, R. Paulo, J. Sacks, J. Cafeo, J. Cavendish, C. Lin, and J. Tu, "A framework for validation of computer models," in "Proceedings of the Workshop on Foundations for V and V in the 21st Century," Society Modeling Simulation Int., San Diego, CA, NISS Tech. Rep. 2002-128, 2002.

[25] B. Ganapol, L. Johnson, C. Hlavka, and D. Peterson, "LEAFMOD: A new within-leaf radiative transfer model," *Remote Sens. Environ.*, vol. 63, no. 2, pp. 182–193, Feb. 1998.

[26] B. Hosgood, S. Jacquemound, G. Andreoli, J. Verdebout, G. Peredrini, and G. Schmuck, *Leaf Optical Properties EXperiment (LOPEX93)*, 1995. Joint Research Center-European Commission, Institute for Remote Sensing Applications, Tech. Rep.

[27] P. Kubelka and F. Munk, "Ein beitrag zur optik der farbanstriche," *Ann. Techn. Phys.*, vol. 11, pp. 593–601, 1931.

[28] R. Clark and T. Roush, "Reflectance spectroscopy–quantitative analysis techniques for remote sensing applications," *J. Geophys. Res.*, vol. 89, no. 10, pp. 6329–6340, Jul. 1984.

[29] S. Jacquemoud and F. Baret, "PROSPECT: A model of leaf optical properties spectra," *Remote Sens. Environ.*, vol. 34, no. 2, pp. 75–91, Nov. 1990.

[30] B. Ganapol, "Vegetation canopy reflectance modeling with turbid medium radiative transfer," in *Computational Methods in Transport*, F. Graziani, Ed. Berlin, Germany: Springer-Verlag, 2006, p. 173.

[31] B. Ganapol and R. Myneni, "The F_n method for the one-angle radiative transfer equation applied to plant canopies," *Remote Sens. Environ.*, vol. 39, no. 3, pp. 213–231, Mar. 1992.

[32] W. Huang, Z. Niu, J. Wang, L. Liu, C. Zhao, and Q. Liu, "Identifying crop leaf angle distribution based on two-temporal and bidirectional canopy reflectance," *IEEE Trans. Geosci. Remote Sens.*, vol. 44, no. 12, pp. 3601–3609, Dec. 2006.

[33] C. Bacour, F. Baret, D. Béal, M. Weiss, and K. Pavageau, "Neural network estimation of *LAI, fAPAR, fCover* and $LAI \times C_{ab}$ from top of canopy MERIS reflectance data: Principles and validation," *Remote Sens. Environ.*, vol. 105, no. 4, pp. 313–325, Dec. 2006.

[34] Z. Jiang, A. Huete, J. Li, and Y. Chen, "An analysis of angle-based with ratio-based vegetation indices," *IEEE Trans. Geosci. Remote Sens.*, vol. 44, no. 9, pp. 2506–2513, Sep. 2006.

[35] R. Salvador, J. Piñol, S. Tarantola, and E. Pla, "Global sensitivity analysis and scale effects of a fire propagation model used over Mediterranean shrublands," *Ecol. Model.*, vol. 136, no. 2/3, pp. 175–189, 2001.

[36] M. McKay, R. Beckman, and W. Conover, "A comparison of three methods for selecting values of input variables in the analysis of output from a computer code," *Technometrics*, vol. 21, no. 2, pp. 239–245, May 1979.

[37] W. Gilks, S. Richardson, and D. Spiegelhalter, Eds., *Markov Chain Monte Carlo in Practice*. London, U.K.: Chapman & Hall, 1995.

[38] N. Goel, "Models of vegetation canopy reflectance and their use in estimation of biophysical parameters from reflectance data," *Remote Sens. Rev.*, vol. 4, no. 1, pp. 1–222, 1988.

[39] J. Clevers and W. Verhoef, "Modeling and synergistic use of optical and microwave remote sensing. LAI estimation from canopy reflectance and WDVI: A sensitivity analysis with the SAIL model," Netherlands Remote Sens. Board (BCRS), Delf, The Netherlands, Tech. Rep. 90-39, 1991.

[40] J. Dungan and B. Ganapol, "Sources of uncertainty in the prediction of LAI/fPAR from MODIS," in *Proc. AGU Fall Meeting*, San Francisco, CA, 2002.

[41] S. Running, D. Baldocchi, D. Turner, S. Gower, P. Bakwin, and K. Hibbard, "A global terrestrial monitoring network integrating tower fluxes, flask sampling, ecosystem modeling and EOS satellite data," *Remote Sens. Environ.*, vol. 70, no. 1, pp. 108–127, Oct. 1999.

[42] W. Cohen, S. Gower, D. Turner, and S. Running, "Linking *in situ* measurements, remote sensing and models to validate MODIS products related to the terrestrial carbon cycle: Boreal forests," *LTER/GTOS Carbon Flux Scaling Workshop*, May 2001, Blue River, OR: HJA Andrews Experimental Forest. [Online]. Available: http://www.fsl.orst.edu/larse/bigfoot/pubs_pres.html

Robin D. Morris (M'01) received the M.A. degree in electrical and information sciences and the Ph.D. degree in signal processing both from Cambridge University, Cambridge, U.K.

He is a Research Scientist with the Universities Space Research Association-Research Institute for Advanced Computer Science, Mountain View, CA. He is also an Associate Adjunct Professor with the Department of Applied Mathematics and Statistics, University of California, Santa Cruz. He was a Postdoctoral Researcher with Institut National de Recherche en Informatique et en Automatique, Sophia Antipolis, France, and with NASA Ames. His research interests are in Bayesian inference for scientific data analysis.

Athanasios Kottas received the Ph.D. degree in statistics from the University of Connecticut, Storrs, in 2000.

He is an Associate Professor with the Department of Applied Mathematics and Statistics, University of California, Santa Cruz. His research interests include Bayesian nonparametric modeling for computer model experiments, regression problems, survival analysis, and spatial statistics, with applications in ecology and engineering.

Matthew Taddy received the B.A. degree in philosophy and mathematics and the M.S. degree in mathematical statistics from McGill University, Montreal, QC, Canada, in 2003 and 2005, respectively, and the Ph.D. degree in statistics and stochastic modeling from the University of California, Santa Cruz, in 2008.

He is an Assistant Professor of Econometrics and Statistics with the Graduate School of Business, University of Chicago, Chicago, IL.

Roberto Furfaro received the Laurea degree (master equivalent) in aeronautical engineering from Universita di Roma La Sapienza, Rome, Italy, in 1998 and the Ph.D. degree in aerospace engineering from the University of Arizona (UA), Tucson, in 2004.

From 1998 to 2002, he was a Researcher with the UA/NASA Space Engineering Research Center. From 2002 to 2004, he was with the Ecosystem Science and Technology Branch, NASA Ames Research Center. Since 2005, he has been an Assistant Research Professor with the Department of Aerospace and Mechanical Engineering, University of Arizona.

Dr. Furfaro is an active member of the Global-Land and Ice Measurement from Space consortium lead by the University of Arizona and a member of the American Geophysical Union.
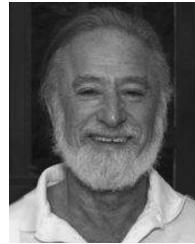
Barry D. Ganapol received the B.S. degree in mechanical engineering from the University of California, Berkeley (UC Berkeley), in 1966, the M.S. degree in engineering science from Columbia University, New York, NY, in 1967, and the Ph.D. degree in nuclear engineering from UC Berkeley, in 1971.

He is currently a Professor with the Department of Aerospace and Mechanical Engineering and with the Department of Hydrology and Water Resources, University of Arizona, Tucson. Over the past 35 years, he has been a Visiting Scientist at Los Alamos National Laboratory, NASA Ames, NASA Goddard, U.S. Airforce Laboratory, Idaho National Laboratory, Oak Ridge National Laboratory, and many universities around the world.

Dr. Ganapol is a Fellow of the American Nuclear Society. In 2006, he was named Da Vinci Fellow at the University of Arizona. In 2005, he was the recipient of the G. Pomraning memorial award.